Title

A novel DDB2 mutation causes defective recognition of UV-induced DNA damages and prevalent equine squamous cell carcinoma

Authors

Chen, Lu
Bellone, Rebecca R
Wang, Yan
et al.

Publication Date

2021

DOI

10.1016/j.dnarep.2020.103022

Peer reviewed

HHS Public Access

Author manuscript

DNA Repair (Amst). Author manuscript; available in PMC 2022 January 01.

Published in final edited form as:

DNA Repair (Amst). 2021 January ; 97: 103022. doi:10.1016/j.dnarep.2020.103022.

A novel DDB2 mutation causes defective recognition of UV-induced DNA damages and prevalent equine squamous cell carcinoma

Lu Chen[a,b,c,*], **Rebecca R. Bellone**[d,e], **Yan Wang**[a,b,c], **Moriel Singer-Berk**[d,e], **Kaoru Sugasawa**[g], **James M. Ford**[b,f], **Steven E. Artandi**[a,b,c]

[a]Stanford Cancer Institute, Stanford University School of Medicine, Stanford, CA 94305, USA

[b]Department of Medicine, Stanford University School of Medicine, Stanford, CA 94305, USA

[c]Department of Biochemistry, Stanford University School of Medicine, Stanford, CA 94305, USA

[d]Department of Population Health and Reproduction, School of Veterinary Medicine, University of California-Davis, Davis, CA 95616, USA

[e]Veterinary Genetics Laboratory, School of Veterinary Medicine, University of California-Davis, Davis, CA 95616, USA

[f]Department of Genetics, Stanford University School of Medicine, Stanford, CA 94304, USA

[g]Biosignal Research Center, Kobe University, Kobe, Hyogo 657-8501, Japan

Abstract

Squamous cell carcinoma (SCC) occurs frequently in the human Xeroderma Pigmentosum (XP) syndrome and is characterized by deficient UV-damage repair. SCC is the most common equine ocular cancer and the only associated genetic risk factor is a UV-damage repair protein. Specifically, a missense mutation in horse DDB2 (T338M) was strongly associated with both limbal SCC and third eyelid SCC in three breeds of horses (Halflinger, Belgian, and Rocky Mountain Horses) and was hypothesized to impair binding to UV-damaged DNA. Here, we investigate DDB2-T338M mutant's capacity to recognize UV lesions *in vitro* and *in vivo*, together with human XP mutants DDB2-R273H and -K244E. We show that the recombinant DDB2-T338M assembles with DDB1, but fails to show any detectable binding to DNA substrates with or without UV lesions, due to a potential structural disruption of the rigid DNA recognition β-loop. Consistently, we demonstrate that the cellular DDB2-T338M is defective in its recruitment to focally radiated DNA damages, and in its access to chromatin. Thus, we provide direct functional evidence indicating the DDB2-T338M recapitulates molecular defects of human XP mutants, and is the causal loss-of-function allele that gives rise to equine ocular SCCs. Our findings shed new light on the mechanism of DNA recognition by UV-DDB and on the initiation of ocular malignancy.

[*]Corresponding author at: Stanford Cancer Institute, Stanford University School of Medicine, Stanford, CA 94305, USA. luchen2@stanford.edu (L. Chen).

Declaration of Competing Interest

RRB directs the Veterinary Genetics Laboratory (University of California-Davis), where a commercial test for the DDB2-T338M mutation in horses is offered.

Keywords

Xeroderma pigmentosum; Squamous cell carcinoma; Equine genetics; Disease mutations; UV-DDB; Localized UV irradiation; Chromatin association

1. Introduction

Ultraviolet (UV) irradiation induces covalent crosslinks between neighboring pyrimidines. If left unrepaired, error-prone replication of this damaged DNA leads to increased rate of mutagenesis and genome instability [1,2]. Specialized damage-surveillance factor UV-DDB recognizes diverse photo-lesions, crucial for the dynamic process of nucleotide excision repair (NER) [3]. Loss of function mutations in the gene encoding the DDB2 subunit of UV-DDB are associated with a rare autosomal recessive syndrome Xeroderma Pigmentosum (XP), which is characterized by sun sensitivity and severe risk for skin cancers [4].

Cellular UV-DDB activity requires two protein subunits, DDB1 and DDB2. DDB2′s WD40 domain provides the sole recognition interface for diverse photo-damage [5], including those buried in nucleosomes [6], whereas DDB1 is needed to facilitate the folding and stability of DDB2 [7]. DDB1 also serves as a substrate adaptor for Cul4 E3 ubiquitination ligase complexes [8,9]. DDB2′s role in UV-DDB seem to reflect a more recent evolutionary adaption to repair UV-lesions: while DDB1 is conserved from fission yeast to human, DDB2′s homologs have only been previously reported in vertebrates [4]. Inactivating DDB2 mutants R273H and K244E have been found in XP complementation group E (XP-E) human patients, whereas no DDB1 mutation has been reported. In addition, UV-DDB is limited by the transcription level of DDB2 mRNA, which is activated by the transcription factor P53 in human cells, but not in rodents, where very low level of UV-DDB can be detected [4].

Squamous cell carcinoma (SCC) is frequently detected among XP patients [10], and is also the most common ocular cancer in horses [11]. We previously studied the Haflinger horse breed with high SCC occurrence of the limbus, and found an autosomal recessive mode of inheritance [12]. A genome-wide association study (GWAS) followed by candidate gene sequencing identified a major genetic risk locus, where a missense mutation T338M of DDB2 gene was found as a candidate SCC allele [13]. Later, the same variant was found to be a risk factor for SCC initiated from the third eye lid, also known as the nictitating membrane [14], and from additional horse breeds [15,16]. This work led to the speculation that this was a loss-of-function variant and a causal risk factor for ocular SCC as computational modeling predicted that this mutation altered conformation of the β loop involved in photolesion recognition [13].

Here, we provide direct functional evidence indicating that the T338M mutant indeed is a loss-of-function allele that abolishes UV-DDB recognition of damaged DNA. We present a structural rationale for T338 to anchor the critical β-hairpin loop of DDB2 for proper DNA-engagement. Our biochemical and cellular characterizations of the T338M and human XP-E mutants prompted us to propose a 2-step damage-scanning model that critically depends on the β-hairpin loop anchored by the T338 residue.

2. Results

2.1. The conserved T338 of DDB2 tightly anchors the DNA-displacing loop of UV-DDB

We constructed a phylogenetic tree based on sequence of DDB2 homologs, and found the human and horse DDB2 protein are more related than the murine counterpart (Fig. 1A). While previously only reported in vertebrates, a blastp analysis allowed us to detect an apparent DDB2 homolog in Arabidopsis thaliana (Q6NQ88), a photosynthesis organism. Thus, alignment of these evolutionarily diverse DDB2 reveals site-specific conservation and divergence within the β-hairpin loop, a crucial DNA-contacting loop connecting the 5th and 6th propeller domains of the WD40 fold of DDB2 (Fig. 1B and C). The tri-residues, F334, N335, and H336, directly contact undamaged DNA bases, forming a DNA-displacing finger [5,17] that are conserved across all species evaluated. While divergence in the rest of loop residues is observed, the T338 is one of the most conserved residues, with 100 % conservation across all seven diverse species examined (Fig. 1B).

The T338 locates spatially at the geometric center of the narrower plane of DDB2′s WD40 barrel, surrounded by other propeller loops (Fig. 1C–E). The T338 tops the DNA-displacing finger protruding downward into the DNA minor groove (colored in blue, Fig. 1C). We hypothesize that the T338 may play an anchorage role for the DNA-displacing finger given its unique positioning. To describe the structural dynamics of T338, the DNA-displacing finger, and other WD40 loops under different biological context, we superimposed available X-ray crystallographic [5,8] or Cryo-EM structures [6] of UV-DDB complexes. Our structure superimposition includes those obtained with diverse origins (zebrafish fish *vs.* human) and composition (dimer *vs.* the CRL4-E3 complex), and with various type of damaged substrates (THF *vs.* 6–4pp) that are embedded in either naked or nucleosomal DNA (Fig. 1D). We found that the β-hairpin loop, including the T338 and the DNA-displacing finger, are spatially constraint in imposed structures, resulting in an invariant conformational consensus. This is unique among other WD40 loops, which show higher levels of conformational heterogeneity. The RMSD (root-mean-square derivation) of every α-carbon atom is rendered onto the superimposed structures in Fig. 1E. The comparison of the average RMSD score for each WD40 loops confirms that T338 resides in the hairpin loop with the highest structural conservation, indicating the DNA-displacing finger maintains high level of structural rigidity irrespective of the complex composition and substrates.

To explore T338′s contribution to the structural rigidity of the hairpin loop, we compared the RMSD value and hydrogen bonding among loop residues. T338 has the lowest RMSD value among all loop residues (Fig. 1F). Furthermore, T338 can form three salt bridges simultaneously with residues in surrounding propellers. The hydroxyl group of T338 interacts with both Arg113 *via* electrostatic interaction (2.9 Å), and with A144 or V114 *via* a hydrogen bond (2.0 Å), as previously predicted [13]. In addition, the backbone oxygen of T338 engages in another hydrogen bond (2.6 Å) with the amid hydrogen of S396′s side chain (Fig. 1F). The DNA-displacing finger is additionally stabilized by an inter-backbone hydrogen bond between L337 and F334 (2.3 Å).

The high affinity, sequence-independent recognition of photodamaged DNA by UV-DDB depends on insertion of the DNA-displacing finger into the DNA minor groove, coupled with simultaneous flipping-out of the damaged base (D2, abasic) and its 3′ neighbor (D1, Fig. 1G and H) [5]. The imidazole ring of H336 becomes coplanar with the undamaged base "Orphan2′′ (marked by an arrow in Fig. 1H) replacing D2. H336 also pi-stacks with the "D3′′ base on the damaged strand. The orphan2 is further stabilized by pi-stacking of its deoxyribose against F334 (Fig. 1H). Furthermore, the carboxamide of Q335 is paired with the base of Orphan1 by hydrogen-bonding (Fig. 1G).

As the immediate adjacent residue with tight spatial constrains, T338 is positioned at the anchor point for this precisely positioned DNA-displacing finger, which is required for damage recognition. Thus, our structural modeling predicts that the T338M mutant might interfere with DNA binding due to loss of hydrogen bonding potential and structural rigidity that are necessary to anchor DNA-displacing residues.

2.2. DDB2-T338M mutant can bind to DDB1 but is defective in DNA-binding

To assess the functional impact of the T338M substitution as predicted by our conservation and computational modeling, we reconstituted human UV-DDB complex containing several DDB2 variants (including the equine T338M) using multi-Bac expression system [18]. DDB2 folds poorly in the absence of DDB1 [9], therefore cDNAs encoding both subunits were cloned into a bi-cistronic targeting vector for baculovirus recombineering [7]. The DDB1 cDNA is fused with an N' terminal FLAG epitope tag that enables the purification of DDB2 variants that are pre-assembled with DDB1 in insect cells (Hi-Five). We indeed detected in FLAG-purified fractions a prominent 110 kDa protein band, and a ~45 kDa species with lower abundance (Fig. 2A).

Several human XPE mutations, including K244E, are mapped to the DDB2-DNA interface [19,20], while others, including R273H, are mapped to the DDB1-DDB2 interface [21,22]. To assess the ability of the T338M DDB2 to assemble with DDB1, we included the XPE mutant R273H as a negative control, which is defective in DDB1-binding [23]. Indeed, DDB2 R273 locates near the larger plain of the DDB2 WD40 fold, but is spatially away from the helix-loop-helix motif of DDB2 that inserts into DDB1 (Fig. 2C). Nonetheless, R111, a loop residue of DDB1, is positioned within 4 Å of DDB2′s R273.

Western blotting of the baculovirus-infected cell lysates confirmed that both DDB2 mutants, T338M and R273H, accumulated in insect cells to a comparable level as WT DDB2 (upper panel, Fig. 2B). We detected similar level of FLAG-DDB1 in all three FLAG-purified fractions. Only WT and T338M DDB2, but not R273H, co-purified with FLAG-DDB1 (lower panel, Fig. 2B). Consistent with the loss of R273H in the complex, the ~45 kDa band in the Coomassie-stained gel is no longer present (far right panel, Fig. 2A). Our result indicates the T338M DDB2 retains normal molecular interaction with DDB1, unlike the XPE mutant R273H.

The reconstitution of T338M-containing UV-DDB allows us to determine T338′s role in DNA binding and UV damage-sensing. We performed EMSA experiments using 30mer DNA containing lesions at the two central thymidine, including a synthetic abasic site, and

mismatches (Fig. 2D), which were previously shown to be substrates for UV-DDB [24]. As a negative control for the DNA binding ability, we additionally generated UV-DDB carrying K244E, another XPE mutants known to compromise DDB2′s DNA binding and specificity for UV-damage [25]. To test whether a substitution of K244 to a bulky residue would also interfere with DNA binding, we also constructed the K244 F mutant. We showed that K244E and K244 F mutants both can co-purify with F-DDB1 at a similar level as for WT (Fig. 2F, upper). Results from the EMSA experiments suggest that WT UV-DDB can readily bind to undamaged DNA, and showed preferential binding to the abasic and mismatched probes (Fig. 2E and F). The UV-DDB-R273H showed no binding activity due to the lack of DDB2. To our surprise, equal or 3x excessive amount of the T338M mutant failed to exhibit any detectable binding activity to all DNA probes tested, phenocopying the K244 F mutant and the XPE mutant K244E (Fig. 2F, lower). Therefore, we demonstrated a severe DNA-binding defect of the T338M-containing DDB2 mutant, which is apparently folded and assembled properly with DDB1.

2.3. DDB2-T338M mutant failed to be recruited to focally irradiated foci in cells

The physiological substrate for UV-DDBs is chromatinized DNA with higher order structure that can not be recapitulated by *in vitro* DNA binding assays [26]. Furthermore, structural insights on UV-DDB-nucleosome have further supported a role for UV-DDBs as a specialized sensor and recognizer to UV damages occluded by chromatin [6]. To further examine DDB2-T338M's ability to recognize photolesions in a cellular context, we utilized a localized UV irradiation assay, whereby focal DNA damages can be introduced to nuclei by UV irradiation through a polycarbonate microfilter [27,28]. Cyclobutane pyrimidine dimers (CPDs) are the major form of photolesions, and can be detected by immunofluorescence (IF)-staining using an anti-CPD antibody [29]. To test the specificity of the microfilter assay, we monitor the IF pattern of CPD staining when Hela cells are irradiated by 200 J/m^2 UVC light under 3 conditions (Fig. 3A). While only background fluorescence is detected when cells were covered with a layer of aluminum foil during the irradiation, we detect a pan-nuclei pattern with ring-shaped nuclei periphery highlighted when cells were directly irradiated through air only. Importantly, cells that irradiated through a 3μM microfilter exhibited robust pattern of CPD foci (ranging from 1 to 8) in all cells examined (Fig. 3A).

We generated Hela cell lines stably expressing C-terminal V5 tagged DDB2 variants, including pcDNA vector-only as a negative control, DDB2-WT as a positive control, and the T338M mutant, alongside with the two human XPE mutant R237H and K244E (Fig. 3B for V5-IF and Fig. 4 for WB). Upon 200 J/m^2 irradiation through a 3μM microfilter without period of recovery, DDB2-WT show nuclear foci formation in all cells examined, while T338M, R237H, and K244E-expressing cells show these variant protein remain evenly distributed throughout nuclei (Fig. 3B). To test whether the focal UV-induced DDB2 foci colocalize with CPD foci, we performed sequential IF procedures that begins with anti-V5 staining, followed by a fixation step, and DNA denaturing by 2 M HCl, and lastly anti-CPD staining. The fixation step is necessary to preserve the IF signal, as the DNA denaturing step destroys most antigen epitopes, while a prolonged DNA denaturing step is necessary for detecting robust CPD IF signals [30,31]. Notably, we observe robust colocalization between

the DDB2-WT foci and the CPD foci (Fig. 3B) that is not detected in the mutants. However, we did confirm that T338M, R237H, K244E variants-expressing cells have a pan-nuclear pattern of DDB2 expression and were indeed focally irradiated at similar efficiency as WT cells. Thus, DDB2-T338M, as well as human XPE mutants, failed to be recruited to focally damaged DNA sites, suggesting the structural integrity of the β-hairpin loop, the proper assembly with DDB1, and the positive-charged WD40 interface with DNA are all independently required for proper recruitment of DDB2 to photolesions *in vivo*.

2.4. DDB2-T338M and human XPE mutants show defect in chromatin association

To further test the cellular distribution of DDB2 variants, we biochemically fractionated cellular proteins into a soluble fraction under low-salt condition, and a chromatin-bound fraction released from high-speed pellets by DNaseI digestion. We also set up parallel experiments with or without UV radiation on all stable cell lines to monitor any UV-dependent alternations in protein abundance. While β-tubulin, an abundant component of cytoskeleton, is readily detected in the soluble fractions by WB (Fig. 4), we were not able to detect any trace of β-tubulin signal in the chromatin-bound fractions. In addition, soluble fractions do not show any UV-dependent alternation in protein level of endogenous UV-DDB and PCNA, an important scaffold protein that has been shown to transit from soluble nucleoplasmic form to chromatin-bound form in order to participate in DNA repair process [32]. However, we observe consistent, UV-dependent elevation of both DDB1 and PCNA level in all of our chromatin-bound fractions (Fig. 4). Meanwhile, DDB2′s abundance in the soluble fractions appears to be downregulated upon UV, except for the K244E variant (Fig. 4). DDB2 has been shown to be subjected to UV irradiation-dependent proteasomal degradation [33]. However, the observation of K244E mutant to be resistant to UV-triggered degradation has been reported using independent methodologies [34]. Notably, only DDB2-WT proteins are detected at significant level in chromatin-bound fraction, while all variants do not appear to show comparable chromatin association with or without UV irradiation. In summary, we show that disruptions of DDB2′s interfaces either with DNA in T338M and K244E, or with DDB1 in R273H compromise DDB2′s ability to stably associate with chromatin, providing additional molecular rationale for the failure of these mutants to support UV-DDB repair.

3. Discussion

Our findings provide direct functional evidence supporting that the T338M missense mutation is the causal risk allele for squamous cell carcinomas from multiple horse breeds and ocular locations [13,15,16, 35]. In addition, our biochemical observations indicate that the proper orientation and rigidity of the DNA-binding hairpin loop of DDB2 is not only critical for recognizing damaged DNA lesions, but also required for basal-level DNA engagement involving contacts with undamaged DNA. We therefore propose a 2-step sequential model to explain how DDB2 utilizes its rigid DNA-displacing loop to gain access to photodamaged DNA (Fig. 5).

In the first damage-scanning step, DDB2 inserts its rigid DNA-displacing loop into the duplex, constantly displaying undamaged bases outward by competing with existing base-

pairings. The resulted widening and/or unwinding of the DNA favorably brings the negatively charged phosphate-backbone in closer proximity to the bottom of the WD40 fold, where16 basic residues reside. Thereby, DDB2 can sustain a low-affinity substrate-scanning mode in the absence of UV lesions (Fig. 5A), which correlates with DDB2′s robust association with chromatin in absence of UV damages (Fig. 4). This is further supported by the defective DNA-binding and chromatin association in the K244E mutant, whereby the charge swapping mutation could compromise the WD40-DNA interface.

In the subsequent damage-recognition step, once a damaged base is displayed by the DNA-displacing loop, an additional specialized damaging-sensing loops would capture the damaged base, contributing additional binding energy necessary to stabilize existing DNA contacts. The translocation of UV-DDB would in turn be stalled by the gain of stability, leading to a high affinity DNA-binding conformation that contributes to stable association to chromatin, and to efficient recruitment to UV-damaged chromatin sites, which enables subsequent recruitment of repair factors [27,36] (Fig. 5B).

The rigid DNA-displacing loop becomes mis-oriented in the T338M DDB2 mutant due to the loss of essential spatial constrains provided by the hydrogen bonding *via* T338′s hydroxyl group, which is absent for Methionine (Fig. 5C). DDB2 with compromised DNA-displacing loop therefore becomes unable to initiate basal DNA-binding mode, resulting in failure to gain stable association with chromatin and to be recruited to the damaged sites as a critical initiator for the repair process, and eventually in carcinogenesis from UV-sensitive tissues in multiple horse breeds (Fig. 5D) [35]. Interestingly, the proposed 2-step model is in agreement with a single-molecule studying on UV-DDB [25], where it was demonstrate that UV DDB inspects DNA for damages by a 3-dimensional scanning mode, and followed by a second phase of stable engagement to damaged sites.

UV-DDB is required to complement NER activity in cells derived from XP-E patients, but is not mechanistically required for *in vitro* reconstituted NER activity using naked DNA substrates [37], highlighting its specialized role in facilitating DNA repairs in chromatinized environment [6]. Our findings reveal a tight coupling between DDB2′s *in vitro* DNA binding activity and its *in vivo* access to photolesions and chromatin among all variants tested, suggesting DDB2′s cellular functions critically depend on its basal affinity toward naked DNA.

Although established as an inactivating XP-E mutation, how the R273H mutant fails to support UV-DDB is unclear [4]. Interfaces of DDB2 with DNA and DDB1 are both crucial for UV-DDB function. The observation that R273 does not participate directly in any of these two interfaces prompted the prediction that R273 contributes to DNA binding by stabilizing the structure of the 4th blade of WD40/DDB2 [5]. Our biochemical purification provides direct evidence that R273H mutant destabilizes the DDB1-DDB2 assembly. Due to the lack of DDB2-R273H from the fraction purified by DDB1, we could not directly study the DNA binding of DDB2-R273H [24]. Our results show that the R273H mutant failed to be localized to focal UV lesions, and that it failed to stably associate with chromatin, suggesting DDB2′s cellular localization and UV-responsiveness rely on its ability to properly assemble with DDB1.

Different reports exploring binding affinity of UV-DDB toward different substrates reached apparently contradictory conclusions. For example, no significant binding was observed toward T-C mismatch, or naked DNA without damage [38], whereas basal level of DNA binding to undamaged DNA, and a preferential binding to mismatched DNA are evident from another study [24]. We do note the variation in DNA length, the type of UV lesion, and the molar ratio of competitive DNA used in these different studies. We did detect a basal level of binding affinity toward undamaged probes from our WT UV-DDB fraction, which is completely abolished with a single T338M mutation that disrupted the rigidity of the DNA-displacing loop. The fact that the T338M mutant assembles with DDB1 with normal efficiency argues against the possibility that the single amino acid substitution has led to a gross misfolding of the DNA-interface of DDB2. The physiological relevance of the displacing loop-dependent basal DNA affinity is supported by our observations that DDB2-WT stably associate with chromatin in the absence of UV irradiation, while T338M could not (Fig. 4).

Dysfunctional telomeres and the ensuing genome instability are major conduits to epithelial malignancy, but lab mice have long telomeres, and reduced level of chromosomal abnormality have been detected in most mice tumors [39]. As a result, epithelial cancers are rare in mice [40]. Additionally, UV-DDB is not detected in many rodent tissues. Perhaps it is not surprising that the adaption of DDB2 protein for DNA-damage repair varies among species depending on behaviors, habitats, anatomical features, and metabolic demands of sun light. Valuable insights can be learnt from genetic and molecular dissection of tumors originated from additional model organisms, including the horse, as the horse shares similar telomere length and oncogenic exposures as humans.

4. Materials and methods

4.1. Plasmid constructs

The pFastBac-Dual plasmid expressing N-terminal FLAG epitope tagged human DDB1 cDNA and untagged human DDB2 cDNA was a generous gift from Kaoru Sugasawa (Biosignal Research Center, Kobe University, Japan). The mammalian expression vector pcDNA3-DDB2-V5/His with Neocycin-resistance was obtained. [27]. T338M, R273H, K244E and K244 F were introduced into the DDB2 cDNA by site-directed mutagenesis reactions (QuikChange II, Agilent). All constructs in this study are in the process for Addgene deposition.

4.2. Baculovirus production and insect cell culture

To generate the recombinant bacmid, pFastBac-Dual plasmids was transformed into DH10BacY bacterial competent cells (Geneva) carrying a bacmid backbone with integrated YFP expression. The transformed cells were plated on blue-white screening plates containing 50 μg/mL Kanamycine, 7 μg/mL Gentamicin, 10 μg/mL tetracycline, 100 μg/mL X-gal, and 1 mM IPTG. White colonies were re-streaked on agar plates, confirmed by genotyping PCR, and inoculated in liquid culture for bacmid purification. Sf9 insect cells growing in 6-well plates (in SF900III medium, at 27°C) were transfected with purified DNA using FuGENE HD (Promega). Supernatant containing the viral stock was harvested 60 h

post-transfected, and amplified in two consecutive passages at a MOI (Multiplicity of Infection) of 0.1 by infecting Sf9 cultured in suspension format. Cell density was maintained between 3×10^5 ~1.5×10^6/mL in SF900III (Gibco). Cell morphology and percentage of YFP positivity were closely monitored. To express recombinant UV-DDBs, 15 mL of twice amplified baculovirus stock was used to infect 400 mL of HiFive insect cell growing in suspension at 1.0×10^6/mL in SF900III medium. HiFive cells upon harvesting 48 h post infection are usually swelled, and 100 % YFP-positive.

4.3. Purification of recombinant UV-DDBs from insect cells

To prepare for the protein extracts, fresh HiFive cell pellets were washed with PBS, and resuspended with 8x vol of Lys450 buffer, containing 20 mM HEPES-NaOH pH 7.9, 450 mM NaCl, 0.5 % Triton X-100, 10 mM KCl, 4 mM $MgCl_2$, 0.2 mM EDTA, 10 % Glycerol, freshly added 0.2 mM DTT, 200 mM PMSF, and Protease Inhibitor Cocktail (P8340 Sigma), on a nutator for 30 min at 4 °C. The extract was then cleared by centrifugation at 28,000 *g* for 30 min at 4 °C. 10 mL of such cleared extract was incubated with 100 μL bed-volume of anti-FLAG agarose beads for at least on a nutator for 4 h at 4 °C. The immunoprecipitated complexes were washed extensive with Lys450. To competitive elute the FLAG bait proteins, 0.25 μg/μl of 3xFLAG peptide was included in the elution buffer (10 mM HEPES-NaOH pH 7.9, 10 % glycerol, 50 mM NaCl, 1.5 mM MgCl2, 0.05 % Triton X-100, and freshly added 0.2 mM DTT, 200 mM PMSF, and Protease Inhibitor Cocktail), and multiple sequential elutions was performed in a thermomixer shaking at 1400 rpm at room temperature. Finally, elutions were filtered through empty chromatography columns (BIO-RAD 7326204). Aliquots snap-froze on dry ice and stored in −80°C freezer.

4.4. Antibodies used in western blotting and immuno-stainings

Anti-human DDB2 was obtained from Cell Signaling Technology (CST, 5416 T); anti-FLAG mouse monoclonal antibody (M2) was obtained from Sigma (F1804); Anti-FLAG EZview FLAG agarose beads were also obtained from Sigma (E6779); Rabbit anti-V5 monoclonal antibody was obtained from CST (13202); Mouse anti-β-Tubulin (D-10) monoclonal antibody was from Santa Cruz (sc-5274); Mouse monoclonal anti-PCNA (PC10) was from CST (2586 T); Rabbit anti-DDB1 polyclonal antibody was from Invitrogen (PA5-34631); Mouse anti-CPD (TDM-2) monoclonal antibody was obtained from Cosmo Bio. Secondary antibodies against Rabbit IgG (Green-colored, IRDye800, cat# 926-32211) and Mouse IgG (Red-colored, IRDye680, cat#926-68070) IgGs were obtained from LiCoR-Odyssey. Donkey anti-mouse IgG conjugated with Alexa Fluor 594, and donkey anti-rabbit IgG conjugated with Alexa Fluor 488 were obtained from the Jackson ImmunoRsearch.

4.5. Electrophoretic mobility shift assay (EMSA)

Synthesized DNA oligos (sequence shown in Fig. 2D) were annealed using the following PCR program: 95 °C for 2 min, gradually cooled to 25 °C over 45 min, and separated by 10 % polyacrylamide gel electrophoresis (PAGE). The double stranded DNA probe was gel-purified and eluted in gel elution buffer, containing 20 mM Tris-HCl (pH 7.5), 0.25 M sodium acetate (pH 5.2), 1 mM EDTA (pH 8.0), 0.25 % SDS, overnight at 4 °C with end-to-end mixing. DNA probe was then purified by isopropanol precipitation. 2 pmol of DNA

probe was end-labeled by T4 polynucleotide kinase in presence of γ-32 P ATP. The labeled probe was purified using Qiagen PCR purification column and stored in −20 °C for up to one month.

10 μL of EMSA reactions were set up on ice containing a buffer of 20 mM HEPES-NaOH (pH 7.9), 50 mM NaCl, 0.02 % NP-40, 0.02 % Triton X-100, 5% Glycerol, 5 mM MgCl2, 0.1 mg/mL BSA, 1 mM DTT, 200 μM PMSF, protease inhibitors, and 0.1 μg/μl poly(dI-dC). Reaction components were combined in following order: recombinant proteins, the reaction buffer, and lastly ~30 fmole of labeled DNA probe. The binding reaction were performed at 30 °C for 40 min, and separated by PAGE (5% 19:1 acrylamide:bis, 0.25x TBE, 1 % glycerol, pre-run at 120 V for 30 min) and run at 120 V in a cold room for 3 h with constant buffer circulation. The gel was dried, then exposed to a phosphor-imager screen, and scanned by a Typhoon scanner. The scanned image was analyzed using TotalLab Quant software.

4.6. Stable hela cell lines

Hela cells were cultured in standard DMEM containing 10 % FBS. pcDNA3-DDB2-V5/His (NeoR) and derivatives were used to reverse-transfect Hela cells using Fugene-HD (Promega). 30 h post-transfection, cells were selected by 400 μg/mL G418 (Geneticin, Gibco) for 9 days, and were maintained in the presence of 100 μg/mL G418.

4.7. Microfilter UV irradiation

For co-IF of DDB2 and CPD, 4×10^4 Hela cells were seeded onto 12 mm coverslips in a 24-well plate, precoated with 20 μg/mL collagen and 1 μg/mL fibronectin in PBS for 1 h at 37 °C. The coverslips were transferred with help of a hooked 30-G needle and a curved tweezer. 2~3 days post-seeding, cells were washed twice with PBS. 3 μM polycarbonate microfilter was cut into a 12 mm circle, pre-wet, and placed on top of 500 μL PBS in a 24-well plate. UVC irradiation was applied with a UVP Hybrilinker Oven (analytikjena) at 200 J/m^2. Immediately prior to irradiation, PBS was gently withdrawn in full using a P1000 pipette to enable a close contact between cells and the membrane, and was applied back to the well immediately post-irradiation. Cells were fixed in 4 % formalin/PBS at room temperature for 10 min, washed twice with PBS, and permeabilized with 0.5 % Triton X-100/PBS on ice, followed by two washes with PBS. Only one coverslip was processed at a time.

4.8. Sequential staining procedure for co-IF of DDB2 and CPD

Cells were washed twice with PBS in the 24-well plate and blocked with 20 %FBS/PBS on a rotating nutator at 37 °C for 30 min. Then, cells were washed three time with 1 mL of PBS, and equilibrate once in 200 μL 5 %FBS/PBS. 1: 500 dilution of the rabbit anti-V5 primary antibody were diluted in 200 μL 5 %FBS/PBS, and incubated on a nutator at 37 °C for 30 min. After PBS washes, secondary antibody (donkey anti-Rabbit AlexFluor488) was applied to the samples similar as the primary antibody. Cells were subsequently washed four times with PBS. To preserve the DDB2 IF signal, cells were re-fixed in 4 % formalin/PBS at room temperature for 10 min, washed twice with PBS, and followed by a dehydration step in 70 % ethanol at room temperature for 10 min. After two PBS washes, cells were incubated in 2 M HCl at room temperature for 10 min. After three PBS washes, cells were re-blocked

and were stained with the mouse anti-CPD antibody following the similar procedure as the first round of staining. Cells were counter-stained with 100 ng/mL of DAPI in PBS for 5 min prior to mounting with Prolong Gold medium. Images were captured by a Leica DM5000 B microscope with 63x oil objective. The images were processed in ImageJ with the Bio-Formats. The montages were generated using FigureJ.

4.9. Fractionation of chromatin-bound proteins upon UV irradiation

Hela cells were growing in 10 cm dishes until confluency under standard condition. For dishes to be irradiated, cells were PBS-washed and aspirated in full, and immediately UVC-irradiated in a UVP Hybrilinker Oven (analytikjena) at 200 J/m^2. Fresh culture medium was immediately replenished to allow cellular responses for 1 h in the tissue culture incubator. Irradiated and control cells were subsequently harvested by trypsinization, and resuspend in a 400 μL low salt NP40 lysis buffer (25 mM HEPES, 150 mM KCl, 1.5 mM $MgCl_2$, 0.5 % NP40, 10 % glycerol, PH adjusted to 7.5 with KOH, with freshly added 1 mM DTT, 200 μM PMSF, and 1:1000 Protease Inhibitor Cocktail [Sigma, P8340]), and placed on a nutator for gentle mixing at 4 °C for 15 min, followed by a centrifugation step at 21,000× *g* for 20 min at 4 °C. After removal of the supernatant in full, the remaining chromatin pellets were completely resuspended by gentle pipetting using 400 μL DNaseI digestion buffer, containing 300 Kunitz units/mL of DNaseI (from bovine pancreas, Sigma DN25), 10 mM Tris-HCl, pH 7.5, 2.5 mM $MgCl_2$, 0.5 mM $CaCl_2$, 10 % glycerol, and freshly added 1 mM DTT, 200 μM PMSF, and 1:1000 Protease Inhibitor Cocktail (Sigma, P8340). The digestion was performed on a nutator rocking at 37 °C for 30 min, followed by a centrifuge step of 21,000 × g for 1 min at 4 °C. Soluble NP40 fractions and DNaseI-released fractions were quantitated using Bradford assays, and 50 μg of total proteins were separated by SDS-PAGE, and analyzed by western blotting. Total proteins were also visualized by Coomassie staining.

4.10. Structural visualization and superimposition

Molecular graphics and analyses were performed with UCSF Chimera (http://www.rbvi.ucsf.edu/chimera/). The RMSD value of superimposed structural model was calculated and rendered graphically using the structural comparison tool- MatchMaker.

4.11. Phylogenic alignment

DDB2 homologs were identified by searching in the UniProt knowledgebase (https://www.uniprot.org/). The amino acid alignment was built using Geneious prime using Clustal Omega. To build the phylogenic tree, pairwise distances were calculated based on the multiple sequence alignment using the Jukes-Cantor distance model. The tree was built using the UPGMA method.

Acknowledgements

The baculovirus-expression construct is a generous gift from Kaoru Sugasawa (Kobe University, Japan). The troubleshooting of the immunostaining procedure received invaluable helps from Adam Freund (Calico inc.). We also thank the discussions and suggestions from labs of James Ford and Gil Chu (Division of Oncology, Stanford University), and assistance from Margo Crausaz (UC-Davis). This work was supported by NIH (AG056575 and CA197563 to S.E.A.). L.C. was supported by a Stanford Cancer Institute Fellowship Award. This work was supported in part by the UC-Davis Center for Equine Health (#16-06) with funds provided by the State of California Pari-Mutuel Fund and contributions by private donors.

References

[1]. Gillet LC, Scharer OD, Molecular mechanisms of mammalian global genome nucleotide excision repair, Chem. Rev 106 (2006) 253–276. [PubMed: 16464005]

[2]. Hauer MH, Gasser SM, Chromatin and nucleosome dynamics in DNA damage and repair, Genes Dev. 31 (2017) 2204–2221. [PubMed: 29284710]

[3]. Hwang BJ, Chu G, Purification and characterization of a human protein that binds to damaged DNA, Biochemistry 32 (1993) 1657–1666. [PubMed: 8431446]

[4]. Tang J, Chu G, Xeroderma pigmentosum complementation group E and UV-damaged DNA-binding protein, DNA Repair (Amst) 1 (2002) 601–616. [PubMed: 12509284]

[5]. Scrima A, Konickova R, Czyzewski BK, Kawasaki Y, Jeffrey PD, Groisman R, Nakatani Y, Iwai S, Pavletich NP, Thoma NH, Structural basis of UV DNA-damage recognition by the DDB1-DDB2 complex, Cell 135 (2008) 1213–1223. [PubMed: 19109893]

[6]. Matsumoto S, Cavadini S, Bunker RD, Grand RS, Potenza A, Rabl J, Yamamoto J, Schenk AD, Schubeler D, Iwai S, et al., DNA damage detection in nucleosomes involves DNA register shifting, Nature 571 (2019) 79–84. [PubMed: 31142837]

[7]. Sugasawa K, The xeroderma pigmentosum group C protein complex and ultraviolet-damaged DNA-binding protein: functional assays for damage recognition factors involved in global genome repair, Methods Enzymol. 408 (2006) 171–188. [PubMed: 16793369]

[8]. Fischer ES, Scrima A, Bohm K, Matsumoto S, Lingaraju GM, Faty M, Yasuda T, Cavadini S, Wakasugi M, Hanaoka F, et al., The molecular basis of CRL4DDB2/CSA ubiquitin ligase architecture, targeting, and activation, Cell 147 (2011) 1024–1039. [PubMed: 22118460]

[9]. Sugasawa K, Okuda Y, Saijo M, Nishi R, Matsuda N, Chu G, Mori T, Iwai S, Tanaka K, Tanaka K, et al., UV-induced ubiquitylation of XPC protein mediated by UV-DDB-ubiquitin ligase complex, Cell 121 (2005) 387–400. [PubMed: 15882621]

[10]. Fassihi H, Sethi M, Fawcett H, Wing J, Chandler N, Mohammed S, Craythorne E, Morley AM, Lim R, Turner S, et al., Deep phenotyping of 89 xeroderma pigmentosum patients reveals unexpected heterogeneity dependent on the precise molecular defect, Proc. Natl. Acad. Sci. U. S. A 113 (2016) E1236–1245. [PubMed: 26884178]

[11]. Strafuss AC, Squamous cell carcinoma in horses, J. Am. Vet. Med. Assoc 168 (1976) 61–62. [PubMed: 1245449]

[12]. Lassaline M, Cranford TL, Latimer CA, Bellone RR, Limbal squamous cell carcinoma in Haflinger horses, Vet. Ophthalmol 18 (2015) 404–408. [PubMed: 25312447]

[13]. Bellone RR, Liu J, Petersen JL, Mack M, Singer-Berk M, Drogemuller C, Malvick J, Wallner B, Brem G, Penedo MC, et al., A missense mutation in damage-specific DNA binding protein 2 is a genetic risk factor for limbal squamous cell carcinoma in horses, Int. J. Cancer 141 (2017) 342–353. [PubMed: 28425625]

[14]. Singer-Berk M, Knickelbein KE, Vig S, Liu J, Bentley E, Nunnery C, Reilly C, Dwyer A, Drogemuller C, Unger L, et al., Genetic risk for squamous cell carcinoma of the nictitating membrane parallels that of the limbus in Haflinger horses, Anim. Genet 49 (2018) 457–460. [PubMed: 29999543]

[15]. Knickelbein KE, Lassaline ME, Bellone RR, Limbal squamous cell carcinoma in a Rocky Mountain Horse: case report and investigation of genetic contribution, Vet. Ophthalmol 22 (2019) 201–205. [PubMed: 30238589]

[16]. Singer-Berk MH, Knickelbein KE, Lounsberry ZT, Crausaz M, Vig S, Joshi N, Britton M, Settles ML, Reilly CM, Bentley E, et al., Additional evidence for DDB2 T338M as a genetic risk factor for ocular squamous cell carcinoma in horses, Int. J. Genomics (2019) 3610965, 2019.

[17]. Yeh JI, Levine AS, Du S, Chinte U, Ghodke H, Wang H, Shi H, Hsieh CL, Conway JF, Van Houten B, et al., Damaged DNA induced UV-damaged DNA-binding protein (UV-DDB) dimerization and its roles in chromatinized DNA repair, Proc. Natl. Acad. Sci. U. S. A 109 (2012) E2737–2746. [PubMed: 22822215]

[18]. Fitzgerald DJ, Berger P, Schaffitzel C, Yamada K, Richmond TJ, Berger I, Protein complex expression by using multigene baculoviral vectors, Nat. Methods 3 (2006) 1021–1032. [PubMed: 17117155]

[19]. Nichols AF, Ong P, Linn S, Mutations specific to the xeroderma pigmentosum group E Ddb- phenotype, J. Biol. Chem 271 (1996) 24317–24320. [PubMed: 8798680]

[20]. Rapic-Otrin V, Navazza V, Nardo T, Botta E, McLenigan M, Bisi DC, Levine AS, Stefanini M, True XP group E patients have a defective UV-damaged DNA binding protein complex and mutations in DDB2 which reveal the functional domains of its p48 product, Hum. Mol. Genet 12 (2003) 1507–1522. [PubMed: 12812979]

[21]. Beecher M, Kumar N, Jang S, Rapic-Otrin V, Van Houten B, Expanding molecular roles of UV-DDB: shining light on genome stability and cancer, DNA Repair (Amst.) 94 (2020) 102860. [PubMed: 32739133]

[22]. He YJ, McCall CM, Hu J, Zeng Y, Xiong Y, DDB1 functions as a linker to recruit receptor WD40 proteins to CUL4-ROC1 ubiquitin ligases, Genes Dev. 20 (2006) 2949–2954. [PubMed: 17079684]

[23]. Hwang BJ, Toering S, Francke U, Chu G, p48 activates a UV-damaged-DNA binding factor and is defective in xeroderma pigmentosum group E cells that lack binding activity, Mol. Cell. Biol 18 (1998) 4391–4399. [PubMed: 9632823]

[24]. Wittschieben BO, Iwai S, Wood RD, DDB1-DDB2 (xeroderma pigmentosum group E) protein complex recognizes a cyclobutane pyrimidine dimer, mismatches, apurinic/apyrimidinic sites, and compound lesions in DNA, J. Biol. Chem 280 (2005) 39982–39989. [PubMed: 16223728]

[25]. Ghodke H, Wang H, Hsieh CL, Woldemeskel S, Watkins SC, Rapic-Otrin V, Van Houten B, Single-molecule analysis reveals human UV-damaged DNA-binding protein (UV-DDB) dimerizes on DNA via multiple kinetic intermediates, Proc. Natl. Acad. Sci. U. S. A 111 (2014) E1862–1871. [PubMed: 24760829]

[26]. Kornberg RD, The molecular basis of eukaryotic transcription, Proc. Natl. Acad. Sci. U. S. A 104 (2007) 12955–12961. [PubMed: 17670940]

[27]. Fitch ME, Nakajima S, Yasui A, Ford JM, In vivo recruitment of XPC to UV-induced cyclobutane pyrimidine dimers by the DDB2 gene product, J. Biol. Chem 278 (2003) 46906–46910. [PubMed: 12944386]

[28]. Katsumi S, Kobayashi N, Imoto K, Nakagawa A, Yamashina Y, Muramatsu T, Shirai T, Miyagawa S, Sugiura S, Hanaoka F, et al., In situ visualization of ultraviolet-light-induced DNA damage repair in locally irradiated human fibroblasts, J. Invest. Dermatol 117 (2001) 1156–1161. [PubMed: 11710927]

[29]. Mori T, Nakane M, Hattori T, Matsunaga T, Ihara M, Nikaido O, Simultaneous establishment of monoclonal antibodies specific for either cyclobutane pyrimidine dimer or (6-4)photoproduct from the same mouse immunized with ultraviolet-irradiated DNA, Photochem. Photobiol 54 (1991) 225–232. [PubMed: 1780359]

[30]. Dutto I, Cazzalini O, Stivala LA, Prosperi E, An improved method for the detection of nucleotide excision repair factors at local UV DNA damage sites, DNA Repair (Amst.) 51 (2017) 79–84. [PubMed: 28185850]

[31]. Guerrero-Santoro J, Levine AS, Rapic-Otrin V, Co-localization of DNA repair proteins with UV-induced DNA damage in locally irradiated cells, Methods Mol. Biol 682 (2011) 149–161. [PubMed: 21057927]

[32]. Scovassi AI, Prosperi E, Analysis of proliferating cell nuclear antigen (PCNA) associated with DNA, Methods Mol. Biol 314 (2006) 457–475. [PubMed: 16673899]

[33]. Rapic-Otrin V, McLenigan MP, Bisi DC, Gonzalez M, Levine AS, Sequential binding of UV DNA damage binding factor and degradation of the p48 subunit as early events after UV irradiation, Nucleic Acids Res. 30 (2002) 2588–2598. [PubMed: 12034848]

[34]. Luijsterburg MS, Goedhart J, Moser J, Kool H, Geverts B, Houtsmuller AB, Mullenders LH, Vermeulen W, van Driel R, Dynamic in vivo interaction of DDB2 E3 ubiquitin ligase with UV-damaged DNA is independent of damage-recognition protein XPC, J. Cell. Sci 120 (2007) 2706–2716. [PubMed: 17635991]

[35]. Knickelbein KE, Lassaline ME, Singer-Berk M, Reilly CM, Clode AB, Famula TR, Michau TM, Bellone RR, A missense mutation in damage-specific DNA binding protein 2 is a genetic risk factor for ocular squamous cell carcinoma in Belgian horses, Equine Vet. J 52 (2020) 34–40. [PubMed: 30903710]

[36]. Fitch ME, Cross IV, Ford JM, p53 responsive nucleotide excision repair gene products p48 and XPC, but not p53, localize to sites of UV-irradiation-induced DNA damage, in vivo, Carcinogenesis 24 (2003) 843–850. [PubMed: 12771027]

[37]. Aboussekhra A, Biggerstaff M, Shivji MK, Vilpo JA, Moncollin V, Podust VN, Protic M, Hubscher U, Egly JM, Wood RD, Mammalian DNA nucleotide excision repair reconstituted with purified protein components, Cell 80 (1995) 859–868. [PubMed: 7697716]

[38]. Fujiwara Y, Inase A, Kawasaki Y, Yoshikawa S, Iwai S, Characterization of the binding of distamycin A to damaged DNA: a comparison with the DNA recognition of the human DDB protein, Nucleic Acids Symp. Ser. (Oxf.) (2006) 235–236.

[39]. Walrath JC, Hawes JJ, Van Dyke T, Reilly KM, Genetically engineered mouse models in cancer research, Adv. Cancer Res 106 (2010) 113–164. [PubMed: 20399958]

[40]. Artandi SE, DePinho RA, Telomeres and telomerase in cancer, Carcinogenesis 31 (2010) 9–18. [PubMed: 19887512]

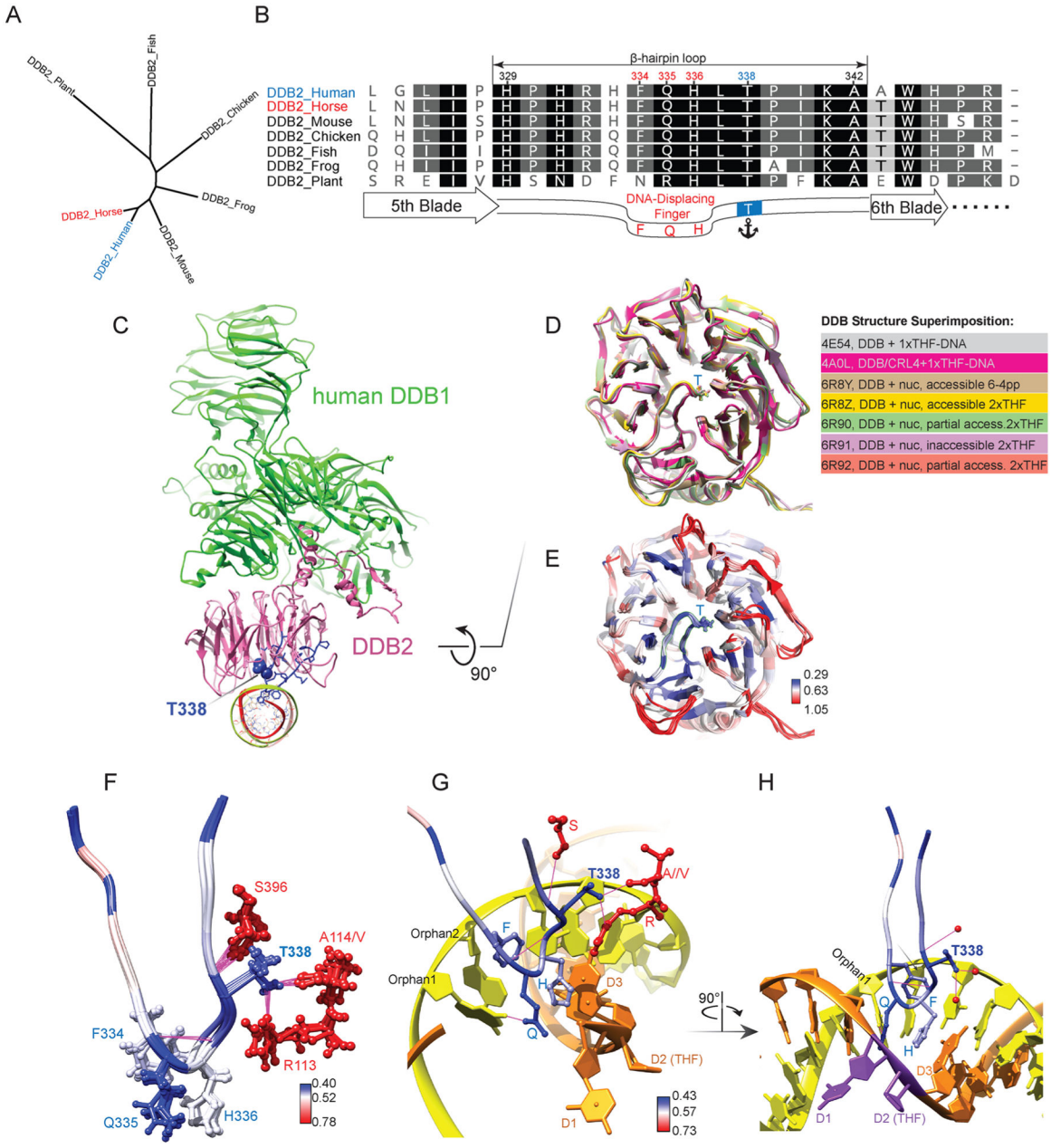

Fig. 1. Structural rationale for T338′s role in anchoring the rigid β-hairpin loop.

(A) An evolutionary tree comparing the phylogenic relationship among DDB2 protein homologs from diverse organisms, including Human (UniProt accession number, Q92466), Horse/*Equus caballus* (F6RQB7), Mouse/*Mus musculus* (Q99J79), Frog/*Xenopus tropicalis* (Q66JG1), Chicken/*Gallus gallus* (Q5ZJL7), Fish/*Danio rerio* (Q2YDS1), and Plant/*Arabidopsis thaliana* (Q6NQ88).

(B) DDB2 homolog alignment of its β-hairpin loop between the 5th and 6th blades of the WD40 domain. β-sheets and the loop were annotated according to DDB2 structures. The T338 (blue) marked by an anchor icon for its proposed role in stabilizing the DNA-displacing residues (Red).

(C) Ribbon representation of the overall UV-DDB dimer complex (4E54): human DDB1, green; human DDB2, pink; The β-hairpin loop, blue; T338′s side chain atoms are shown as blue spheres.
(D) (rotated by 90° along the horizontal axis relative to C, viewing form the bottom of DDB2-WD40) Multiple structural superimposition of DDB2-WD40 domains, in complex with DDB1 or DDB1-CUL4-RBX1 E3 Ligase complex, and with diverse substrates as indicated in the legend; "+nuc", with nucleosomal DNA; accessibility to damaged bases is occluded by histone-DNA contacts, which tolerate DNA damages [6]. PDB IDs are listed.
(E) Similar superimposed view as in D. backbone of residues are rendered according to the RMSD value of each alpha carbon, the corresponding color key for the RMSD is shown.
(F) B-hairpin loop-only view from superimposed structures in E, rendered based on the RMSD color key. The side chain of the DNA-contacting bases and T338 are shown. Other DDB2 residues involved in hydrogen bond (pink lines) are colored in Red.
(G) Close-up of the damage-binding pocket depicting contacts that stabilizing the DNA-displacing finger. All involved side chains are labeled as in F. Undamaged strand, yellow; damaged strand, orange. One of the two flipped-out bases, D2 - the abasic site-mimic containing tetrahydrofuran (THF); The other flipped out base 3′ to D2, namely D1; the base-paired 5′ neighbor to D2, D3. Two orphan bases on the undamaged strand are labeled, Orphan 1 being the 5′ base to Orphan 2.
(H) (rotated by 90° along the vertical axis from G) DNA-displacing residues are coplanar and base-pairing with the two orphan bases (Orphan2 by an arrow), while displacing/flipping the damaged bases D1 and D2 (colored in purple). Atoms of S396, A114, and R113 forming hydrogen bonds with T338 are shown in Red.

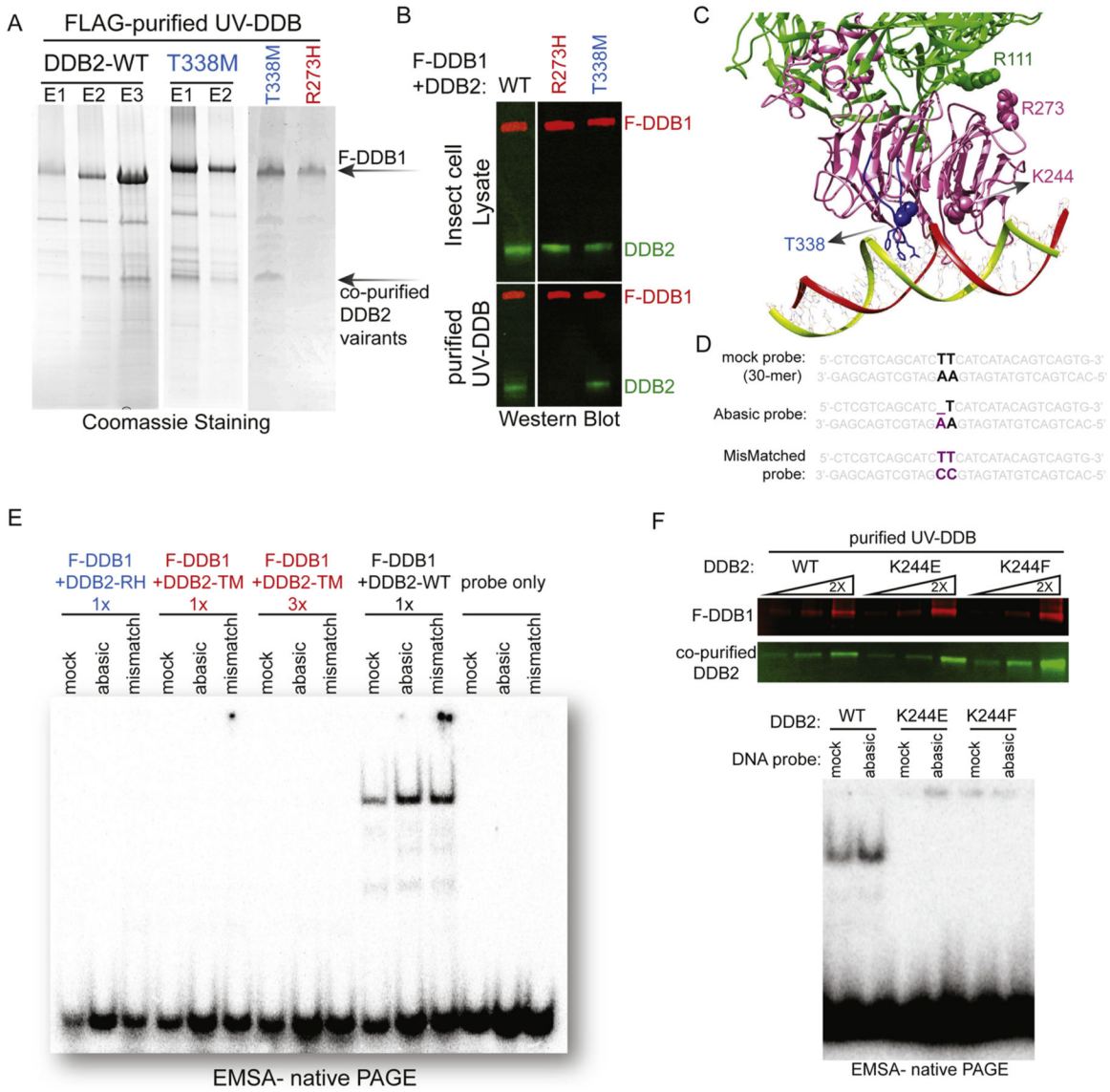

Fig. 2. T338M-DDB2 failed to show DNA-binding activity while can assemble with DDB1.

(A) Reconstituted UV-DDB dimers containing DDB2 mutant T338M and the XPE mutant R273H. Coomassie-stained SDS-PAGE showing fractions of FLAG immunoprecipitations. Input, the Hi-Five insect cell extracts expressing FLAG tagged human DDB1 and untagged DDB2. FT, flow-through extract post-FLAG IP. Purified UV-DDBs were eluted from anti-FLAG resin by competitive FLAG peptide elution sequentially, as in E1, E2, E3.

(B) Western blotting of similar fractions in A. Red signal was originated from anti-FLAG antibody; Green, anti-human DDB2 antibody.

(C) Overall structural representation of UV-DDB highlighting the location of T338 and R273. Side chains of R111 of DDB1, R273, T338, and K244 of DDB2 are shown as spherical models.

(D) Three different DNA substrate probes (30-mer) used as in E and F. The central thymidine dimer position shown in bold. Abnormally base-paired bases shown in purple.

(E) Electrophoretic Mobility Shift Assay (EMSA) reactions separated on a native PAGE. Shifted band represents P^{32}-labeled DNA probes bound by UV-DDB. Unbound band shown near the bottom of the gel. Protein loading in each reaction was normalized by western blotting signal of F-DDB1 as 1 × . For 3x, 3-fold loading of DDB1 containing UV-DDB for the T338M mutant, which did not yield detectable binding.

(F) Characterizations of UV-DDBs containing DDB2-K244E and K244 F that purified by F-DDB1. Western blotting shows comparative level of co-purified DDB2′s as in WT (upper); EMSA (lower) as in E shows undetected DNA binding activity of K244E, and K244 F, compared to WT.

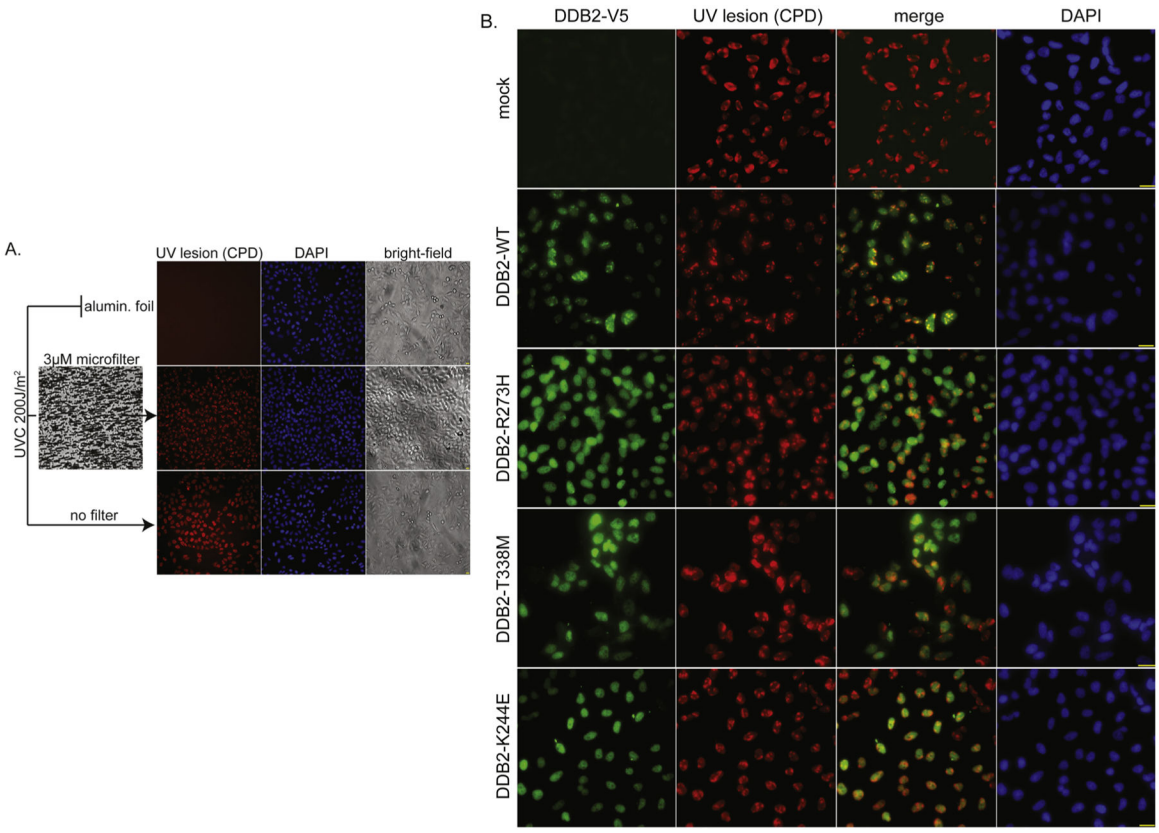

Fig. 3. *In vivo* recruitment of DDB2 with different variants to CPD photolesions.

(A) Evaluate the specificity and prevalence of CPD foci under three parallel conditions: Hela cells were i) covered with a layer of aluminum foil; ii) topped with a 3 μM polycarbonate microfilter; iii) with nothing but air. Cells were irradiated under 200 J/m^2 UVC light, and fixed immediately, followed by 2 M HCl treatment and a blocking step. The CPD signal is visualized by IF using an anti-CPD antibody (red), counterstained by DAPI (blue). A 20x objective was used. Yellow scale bars denote for 20 μM.

(B) Colocalization of DDB2 variants with CPD foci by co-IF. Hela cells stably expressing the indicated DDB2 constructs or mock (vector only) were irradiated through a 3 μM polycarbonate microfilter under 200 J/m^2 UVC light, and fixed immediately for co-IF. Transgenic DDB2-V5 variants were visualized by the anti-V5 antibody (Green), CPD foci in Red. Green and Red channels were overlayed to show colocalization of CPD with DDB2 in "merge". DAPI counter staining in Blue. A 63x oil objective was used. Yellow scale bars denote for 20 μM.

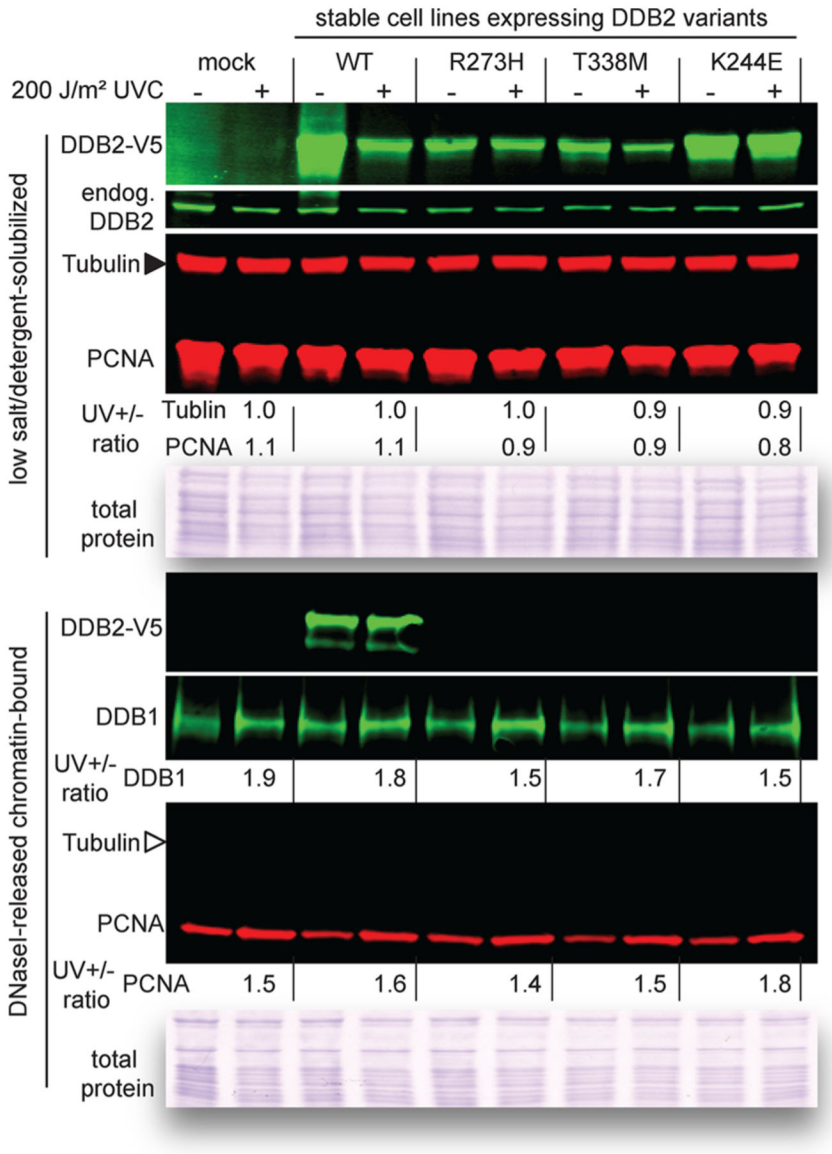

Fig. 4. Biochemical fractionations to enrich chromatin-bound DDB2 variants with or without UVC irradiation.

Hela cell line stably expressing vector only or indicated DDB2-V5 constructs were fractionated into “low salt-detergent-solubilized” and “DNaseI-released chromatin-bound” fractions (see methods), under 200 J/m^2 UVC (+) or without (−). Western Blottings were performed on these fractions with indicated antibodies. Transgenic DDB2-V5 expression was detected using an anti-V5 antibody, while endogenous DDB2 with lower mobility can be detected using an anti-DDB2 antibody. The blots of Tubulin and PCNA for both fractions were blotted back-2-back, and were shown under similar exposure using LiCoR odyssey scanning system. The solid or empty triangle denotes β-tubulin and its expected mobility, which is undetectable in the chromatin-bound fractions even under the most sensitive exposure. UV +/− ratio of indicated antibodies was calculated using the quantitative values

of the irradiated samples divided by mock samples. “total protein” presents Coomassie-stained gel to reflect protein loadings across fractions.

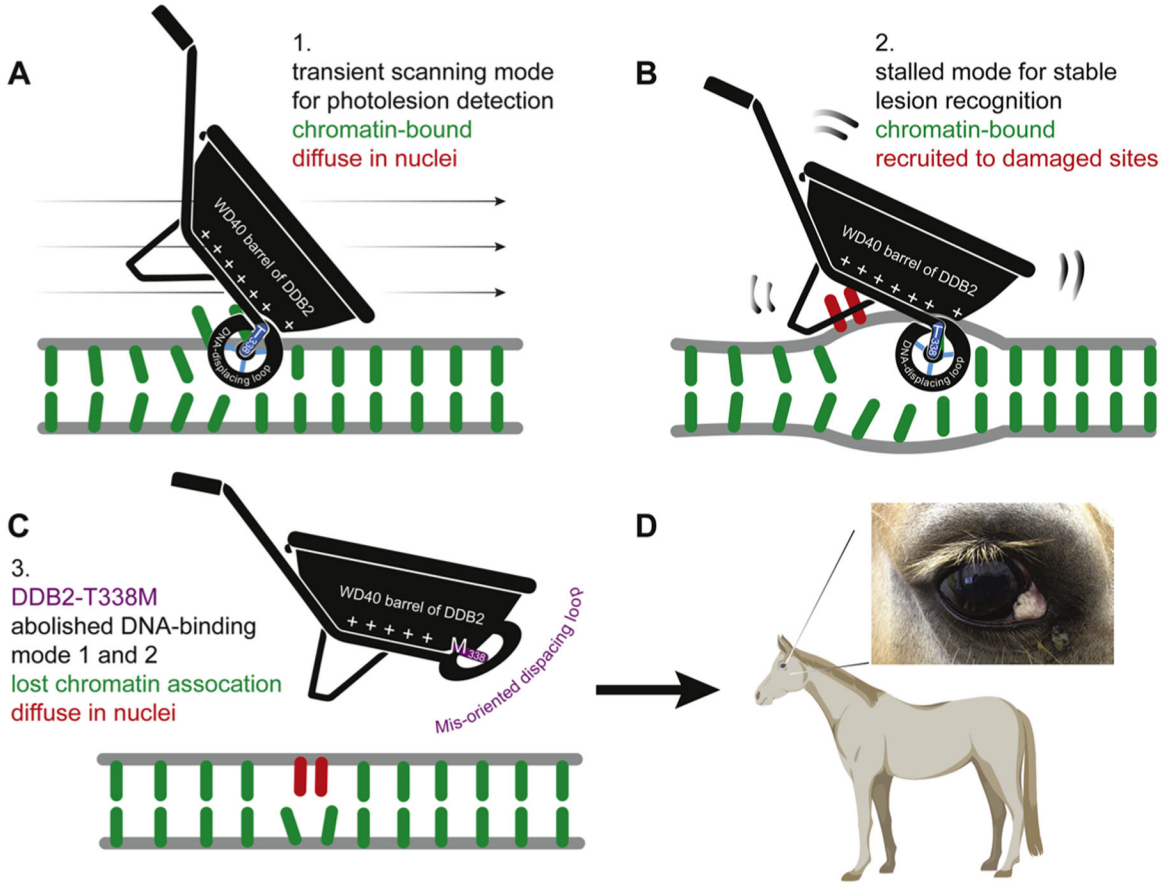

Fig. 5. A 2-step sequential model explaining how DDB2 depends on its rigid DNA-displacing loop to stably recognize photo-lesions.

The WD40 β-barrel is depicted as the basin of a wheelbarrow, whose narrower end represents the DDB2-DNA interface with basic residues lining at the bottom of the basin. The tire of the wheel represents the structurally rigid DNA-displacing loop, whose shape and orientation is supported and maintained by spokes and a central hub (both colored in blue), depicting T338-mediated spatial anchorage and structural stabilization (Fig. 3 A and B). The methionine substitution for the T338 (colored in purple) is depicted as a deformed tire without spokes and hub, so that it no longer can be inserted into the DNA ladder, thereby incapable to initiate basal DNA binding and the 1 st scanning step (Fig. 3A). Regular DNA bases in green, and UV-crosslinked thymidine dimer in red, which is caught by a damaging-recognition loop, depicted by the triangular leg support of the wheelbarrow (Fig. 3B). This 2nd stalled mode further stabilizes the high affinity conformation needed for downstream recruitment of protein repair factors. Lastly, an illustration of an equine squamous cell carcinoma case of the third eyelid, resulting from the loss-of-function and cancer-causing mutation T338M in DDB2.